# Supporting Information

## Harig and Simons 10.1073/pnas.1206785109

### SI Text

**Determination of Noise.** Gravity Recovery and Climate Experiment (GRACE) data are released as spherical harmonic coefficients along with calibrated errors that represent the diagonal elements of the covariance matrix of the estimated global monthly solutions. It is known that these calibrated errors underestimate the variance in GRACE solutions (1) and that monthly solutions are dominated by north–south trending linear stripe anomalies (2). Thus, many studies estimate their own uncertainty for their modeling (3) and attempt to remove estimated noise components (2, 4).

In practice, there is little reason to think that time-variable geopotential signals are best estimated from basis functions that spread their energy over the entire globe. For instance, processes that act in different locations at different times (e.g., monsoons) could easily display competing effects in the same spherical harmonic coefficient. Thus, in our determination of noise specifically over Greenland, we estimate signal and noise in the Slepian basis to avoid contamination from other regions. However, to illustrate the importance of estimating the noise covariance and accounting for it in the subsequent analysis, the global spherical harmonic analysis performed here provides a convenient example. This method of estimating the noise in GRACE data from the spherical harmonic coefficients was first used in the work by Wahr et al. (3) and has subsequently been used in a great many of GRACE studies.

Here, we examine each spherical harmonic coefficient individually as it varies over time, and we find a least squares estimate of a linear term and a seasonal term with a 365-d period. We consider this fit to be an estimate of the signal contained in the GRACE data, and the residuals form a conservative estimate of the noise. Fig. S1, which examines the coefficients spectrally, shows the results of this procedure. Fig. S1*A* shows a single monthly solution of GRACE data for February of 2010. Fig. S1*C* shows the prediction of the signal component for this month. Fig. S1*D* shows the residual after subtracting the signal from the data. Generally, the prediction is dominated by energy in coefficients with degrees less than 30. Meanwhile, the residual has some energy at low-degree coefficients, but it is mainly comprised of energy in coefficients where the order $m$ (and degree $l$) is $-30 \gtrsim m \gtrsim 30$. This result corresponds to the higher-frequency north–south-oriented stripes commonly observed. Finally, Fig. S1*B* shows the SDs of these residual coefficients over all of the months considered. We have made the implicit assumption that the noisy stripes seen in GRACE monthly data are related to the satellite orbit characteristics specific to each month considered, and therefore, these stripes should not have a coherent secular expression over time.

**Covariance of the Noise.** We use the spherical harmonic coefficient residuals from each month to construct a covariance matrix (Fig. S2, shown as a correlation matrix). The residual correlation matrix shows many off-diagonal terms with large correlations. This finding is contrary to what is normally assumed by other works, which examine only the diagonal elements of this matrix (the variance) and assume that the off-diagonal terms are zero.

These large covariance terms make important contributions to the observed spatial covariance on the sphere. In Fig. S3, we show the difference in spatial covariance when the full spectral covariance matrix or only the variance (its diagonal elements) is being used. We consider the covariance between a point in central Greenland and all of the other points on the Earth, and we do the same with a point in western Antarctica.

Additionally, in Fig. S4, we show how our spatial variance compares with the calibrated errors distributed with the monthly geopotential solutions. Most notably, our spatial variance has significant longitudinal dependence compared with the calibrated errors, while also displaying somewhat higher values of SD than the calibrated errors. It is clear that, without the use of the full covariance matrix, estimates of the error in mass change results may be inaccurate. By taking a conservative estimate of the full noise covariance of the data into account, we can have high confidence in our mass estimates compared with the results derived from other techniques.

**Spherical Slepian Basis.** Given that (*i*) time-variable gravity signals often originate in specific regions of interest (*ii*), our data are discreetly measured and therefore, have a band limit, and (*iii*) we may wish to exclude some portion of the spectrum where the error terms are expected to dominate, then we desire an orthogonal basis on the sphere that is both optimally concentrated in our spatial region of interest and band-limited to a chosen degree. For this purpose, we use the spherical analog to the classic Slepian concentration problem (5–8) and define a new set of basis functions (Eq. **S1**):

$$g_\alpha(\hat{\mathbf{r}}) = \sum_{l=0}^{L} \sum_{m=-l}^{l} g_{\alpha,lm} Y_{lm}(\hat{\mathbf{r}}), \quad g_{\alpha,lm} = \int_\Omega g_\alpha(\hat{\mathbf{r}}) Y_{lm}(\hat{\mathbf{r}}) d\Omega. \quad \textbf{[S1]}$$

These functions maximize their energy within our region of interest $R$ following (Eq. **S2**)

$$\lambda = \frac{\int_R g_\alpha^2(\hat{\mathbf{r}}) d\Omega}{\int_\Omega g_\alpha^2(\hat{\mathbf{r}}) d\Omega} = \text{maximum}, \quad \textbf{[S2]}$$

where $1 > \lambda > 0$. The Slepian coefficients, $g_{\alpha,lm}$, are found by solving the eigenvalue equation (Eq. **S3**)

$$\sum_{l'=0}^{L} \sum_{m'=-l'}^{l'} D_{lm,l'm'} g_{l'm'} = \lambda g_{lm}, \quad \textbf{[S3]}$$

where the elements of $D_{lm,l'm'}$ are products of spherical harmonics integrated over the region $R$ (Eq. **S4**):

$$\int_R Y_{lm} Y_{l'm'} \, d\Omega = D_{lm,l'm'}. \quad \textbf{[S4]}$$

The Slepian basis is an ideal tool to conduct estimation problems that are linear or quadratic in the data (8, 9). The data can now be projected into this basis as (Eq. **S5**)

$$d(\hat{\mathbf{r}}) = \sum_{\alpha=1}^{(L+1)^2} d_\alpha g_\alpha(\hat{\mathbf{r}}) = \sum_{l=0}^{L} \sum_{m=-l}^{l} d_{\alpha,lm} Y_{lm}(\hat{\mathbf{r}}) \quad \textbf{[S5]}$$

and by using a truncated sum up to the spherical Shannon number (Eq. **S6**),

$$N = (L+1)^2 \frac{A}{4\pi}, \quad \textbf{[S6]}$$

where $A/4\pi$ is the fractional area of localization to $R$, we can sparsely approximate the data, yet with very good reconstruction properties within the region (10) (**S7**):

$$d(\hat{\mathbf{r}}) \approx \sum_{\alpha=1}^{N} d_\alpha g_\alpha(\hat{\mathbf{r}}) \quad \text{for} \quad \hat{\mathbf{r}} \in R. \qquad \textbf{[S7]}$$

This procedure is analogous to taking a truncated sum of the singular-value decomposition of an ill-posed inverse problem (10). Because the illposedness is, in part, derived from the focus on the limit area of interest, our procedure in effect determines the singular vectors of the inverse problem from the outset based on purely geometric considerations, which is efficient.

We solve for a Slepian basis for Greenland (Fig. S5) up to the same degree and order of the available GRACE data (thus, the bandwidth $L = 60$). We use the coastlines of Greenland and extend them by 0.5° to create the region of concentration $R$. With truncation at the Shannon number $N$, the basis has 20 Slepian functions localized to the region, with the 12th best function (Fig. S5) still concentrated to $\lambda = 86.9\%$.

The Slepian functions are smoothly varying across the land–ocean boundary, and as a result, they can have reduced sensitivity near this boundary. This result is why we extended the concentration region by buffering away from the coastlines. The size of the buffer zone was based on experiments to recover a synthetic mass trend placed uniformly on Greenland's landmass (Fig. S6). In Fig. S6*A*, we show the results of an experiment where a uniform synthetic signal is placed over Greenland, and we attempt to recover this trend. To replicate the experimental conditions faced by the researchers on the ground, we add synthetic realizations of the noise generated from our empirical covariance matrix to this synthetic signal. The signal is best recovered when the region of localization is extended away from the coastlines by 0.5°. This buffer region allows us to better measure mass changes near the coastlines of Greenland, but it is small enough to eliminate influence by mass changes outside of Greenland, such as in Iceland or Svalbard. In Fig. S6*B*, we show how the actual recovered mass trends over Greenland vary depending on the bandwidth and buffer (i.e., region) chosen. Roughly the same trend is recoverable for a broad combination of bandwidth and region buffer; however the lower bandwidths will have reduced spatial sensitivity around Greenland.

**Analysis in the Slepian Basis.** We project each monthly GRACE field, which we convert to surface density, into the Slepian basis for Greenland, which results in a time series for each Slepian expansion coefficient. For each of our 20 Slepian coefficients, we fit a first-, second-, or third-order polynomial to the time series in addition to a 365-d period sinusoidal function, depending on whether each additional polynomial term passes an $F$ test for significance. These quadratic and cubic terms represent the interannual changes in the GRACE data over the data time span. Examples of these fits are shown in Fig. S7. Here, we show the time series of some coefficients and their best-fitting functions, where the fitted annual periodic function has been subtracted. Some time series, such as for $\alpha = 20$, are best represented by a higher-order polynomial, whereas others, such as $\alpha = 11$, are fit by a linear function, because higher-order terms do not significantly reduce variance.

The mass change for an average year, shown in Fig. S8, is found by taking the total estimated mass change from 2003 to 2010 and dividing by time considered. Most of the mass change of this period projects into the first five Slepian functions; however, the remaining 15 functions of the basis are also important to fully capture the spatial pattern of mass change, even if their mass integrals do not form a large part of the total.

After fitting estimated signals in the Slepian domain, the monthly residuals can be used to form an empirical covariance matrix for the Slepian functions (Fig. S2*B*). This information not only gives us estimates for the uncertainty of the signal estimates for each Slepian function but also allows us to determine the overall trend uncertainty for all of Greenland by combining the variance and covariance in error propagation. Using the full covariance information allows us to have high confidence in our trend estimation, more than we felt comfortable with in previous work.

Finally, we can examine the time series for the three most-contributing Slepian functions, which Fig. S9 expresses as the integral of the product of the expansion coefficient and the function. It is clear from this behavior function that the mass signal trends can be well-estimated relative to the variance seen from month to month. The Slepian functions significantly enhance signal to noise within the region of interest compared with traditional spherical harmonics, which further validates our approach.


1. Horwath M, Dietrich R (2006) Errors of regional mass variations inferred from GRACE monthly solutions. *Geophys Res Lett* 33:L07502.
2. Swenson S, Wahr J (2006) Post-processing removal of correlated errors in GRACE data. *Geophys Res Lett* 33:L08402.
3. Wahr J, Swenson S, Velicogna I (2006) Accuracy of GRACE mass estimates. *Geophys Res Lett* 33:L06401.
4. Chen JL, Wilson CR, Tapley BD, Blankenship D, Young D (2008) Antarctic regional ice loss rates from GRACE. *Earth Planet Sci Lett* 266:140–148.
5. Slepian D (1983) Some comments on Fourier analysis, uncertainty, and modeling. *SIAM Rev Soc Ind Appl Math* 25:379–393.
6. Wieczorek MA, Simons FJ (2005) Localized spectral analysis on the sphere. *Geophys J Int* 162:655–675.
7. Simons FJ, Dahlen FA, Wieczorek MA (2006) Spatiospectral concentration on a sphere. *SIAM Rev Soc Ind Appl Math* 48:504–536.
8. Simons FJ, Dahlen FA (2006) Spherical Slepian functions and the polar gap in geodesy. *Geophys J Int* 166:1039–1061.
9. Dahlen FA, Simons FJ (2008) Spectral estimation on a sphere in geophysics and cosmology. *Geophys J Int* 174:774–807.
10. Simons FJ (2010) *Handbook of Geomathematics*, eds Freeden W, Nashed MZ, Sonar T (Springer, Berlin), pp 891–923.

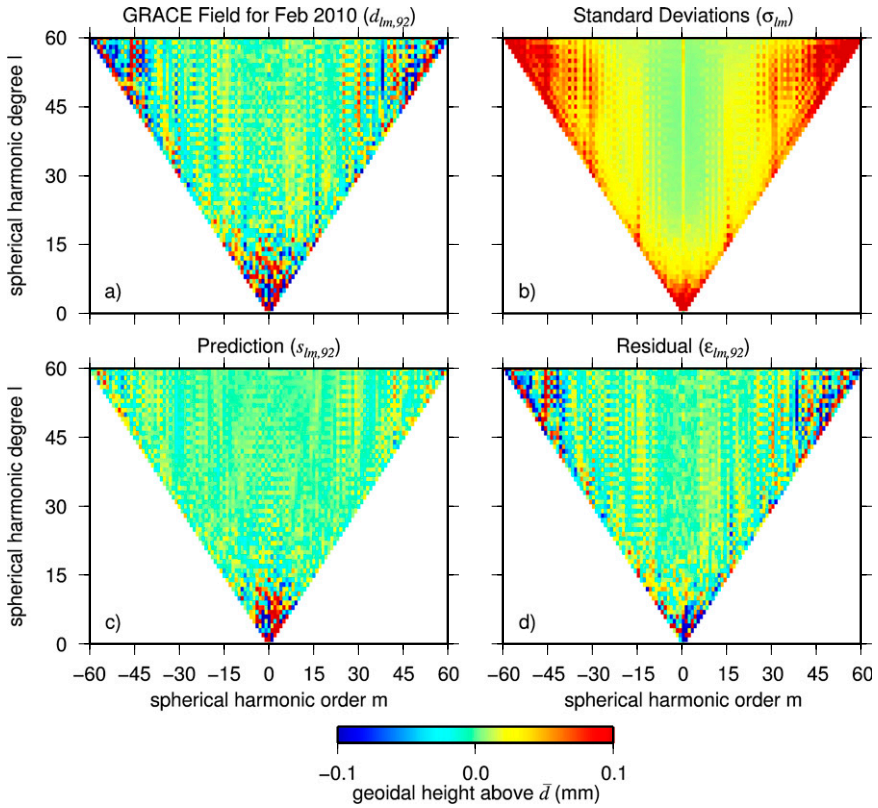


**Fig. S1.** Ordered maps of various spherical harmonic coefficients. (*A*) The geoidal coefficients ($d_{lm,92}$) of GRACE data from February of 2010 after the average of all data months has been removed. (*B*) SDs ($\sigma_{lm} = [1/M\sum_{n=1}^{M} d_{lm,n}]^{1/2}$ for months $n = 1, \ldots, M$, where $n = 92$ stands for February of 2010) of the residuals as estimated by subtracting the least squares fits comprising a linear and two seasonal terms with periods 365 and 181 d from each time series of geoidal spherical harmonic coefficients and computing the covariance of the results. (*C*) The predicted geoidal coefficients ($s_{lm,92}$) from the least squares model fit as described before in *B*. (*D*) The residual geoidal coefficients ($\epsilon_{lm,92} = d_{lm,92} - s_{lm,92}$) were determined by subtracting the predicted coefficients (*C*) from the GRACE geoidal field (*A*).

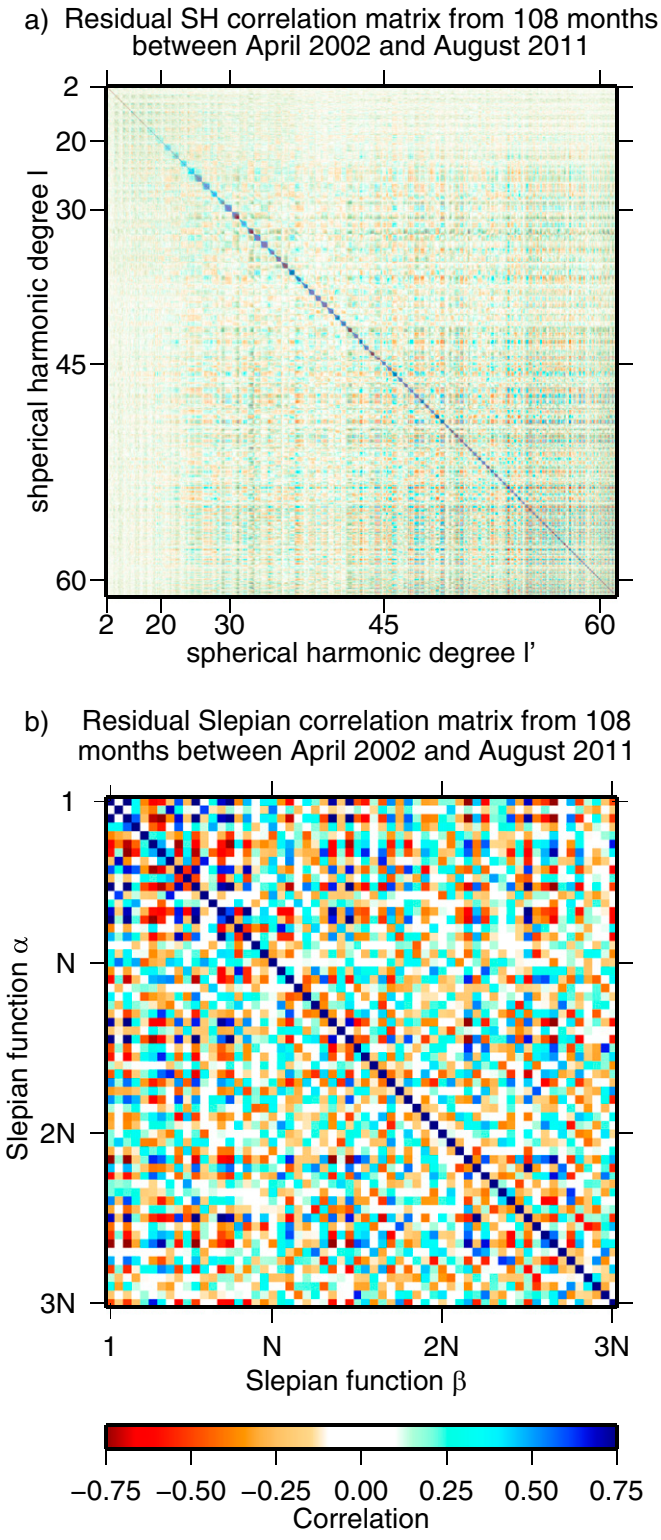


**Fig. S2.** Correlation matrices for spherical harmonic and Slepian coefficients created from the residuals of 108 mo from April of 2002 to August of 2011. (*A*) Correlation between spherical harmonic coefficients derived from the spectral covariance cov[$\varepsilon_{lm}$, $\varepsilon_{l'm'}$]. (*B*) Correlation between Slepian function coefficients for a basis for Greenland with a region buffer of 0.5° and a bandwidth $L = 60$. The rounded Shannon number is $n = 20$.

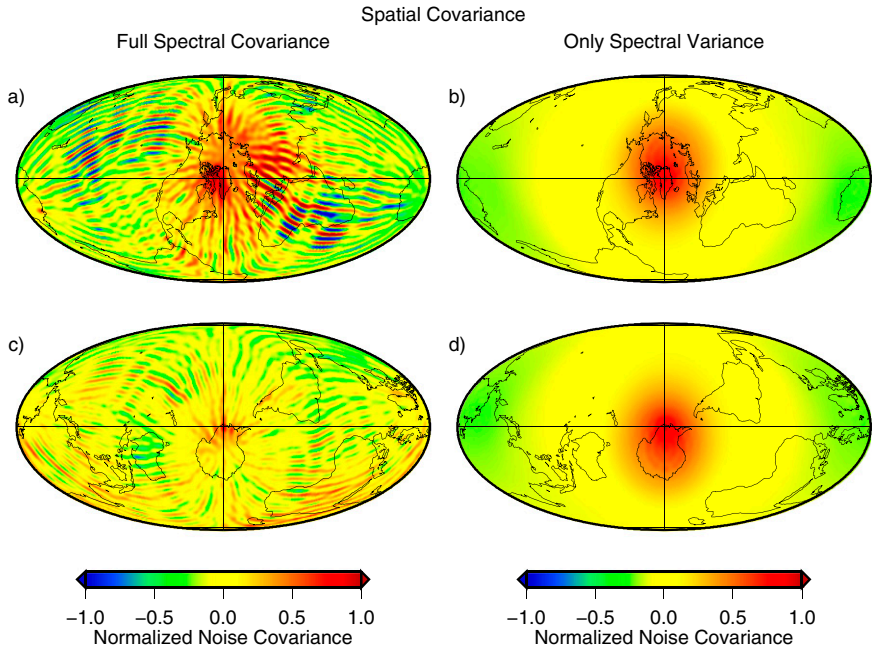


**Fig. S3.** Spatial covariance plots of residuals, cov[$\varepsilon_r$, $\varepsilon_{r'}$]. Fields have been rotated, and therefore, the central cross denotes the point r with which all of the other points r′ covary. In *A* and *C*, the full spectral covariance matrix is used. *B* and *D* use only the spectral variance and the diagonal elements of covariance matrix. (*A* and *B*) The covariance of a point in Greenland with the rest of the Earth. (*C* and *D*) Covariance of a point in western Antarctica with the rest of the globe.

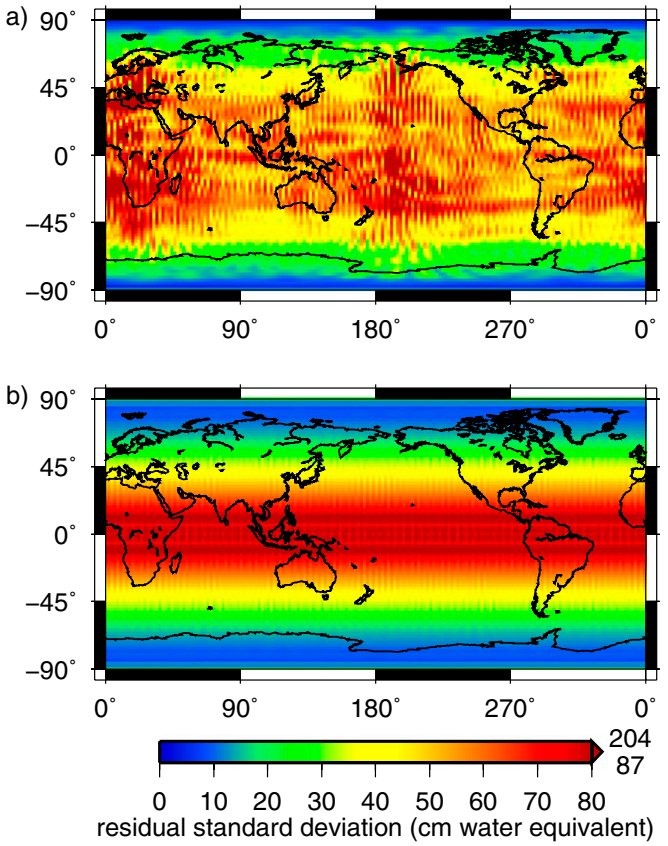


**Fig. S4.** (*A*) Spatial SD from our full spectral estimated covariance matrix, and (*B*) SD using only the spectral variance (diagonal) terms of the covariance matrix (off-diagonal terms are set to zero). Both plots are saturated at 80 cm water equivalent, but *A* and *B* have the denoted maximums of 204 and 87 cm, respectively.

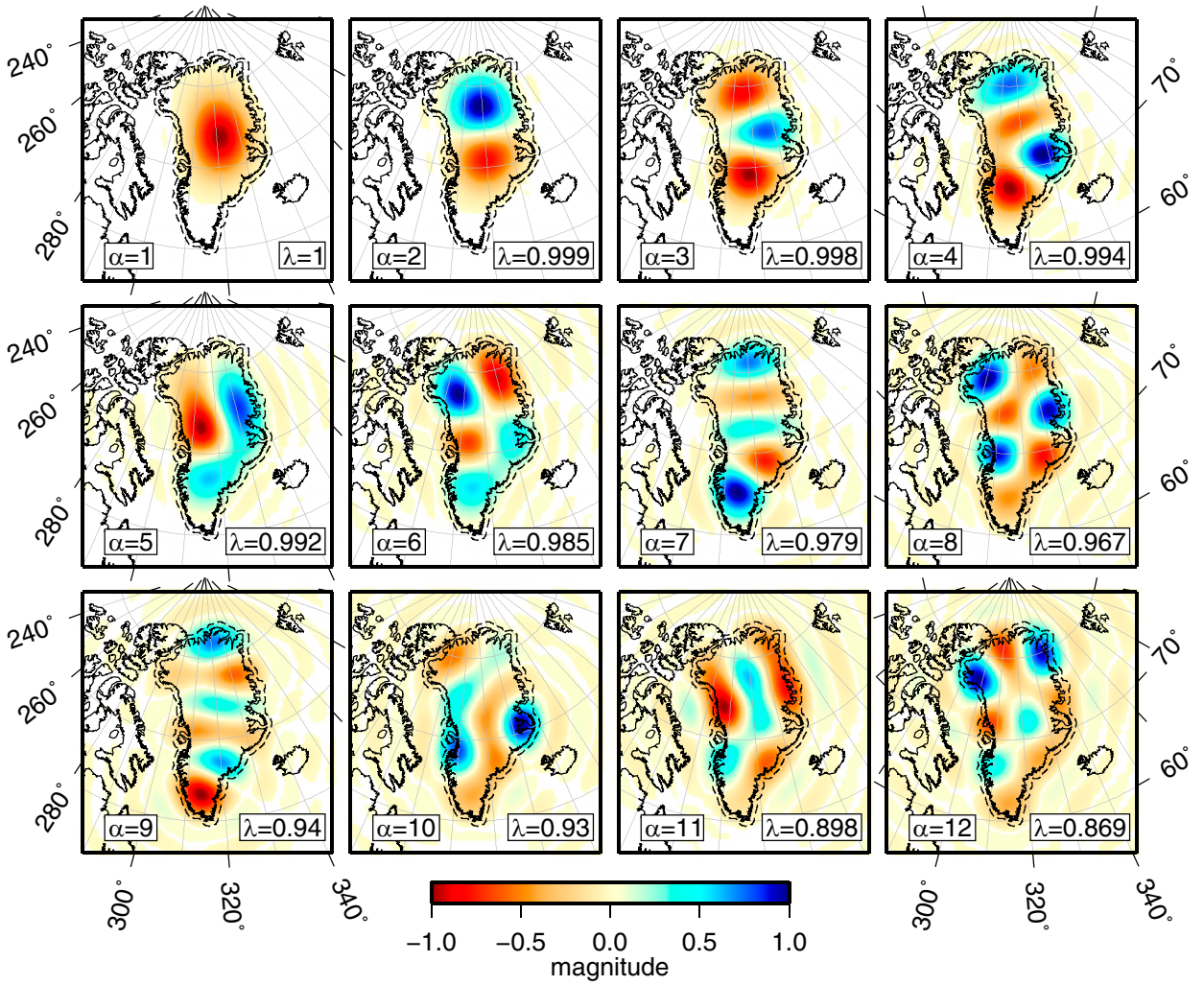


**Fig. S5.** Slepian eigenfunctions $g_1$, $g_2$, ..., $g_{12}$ that are optimally concentrated within a region buffering Greenland by 0.5°. The dashed lines indicate the regions of concentration. Functions are band-limited to $L = 60$ and scaled to unit magnitude. The parameter $\alpha$ denotes the eigenfunction that is shown. The parameter $\lambda$ is the corresponding eigenvalue for each function, indicating the amount of concentration. Magnitude values with absolute values that are smaller than 0.01 are left white.

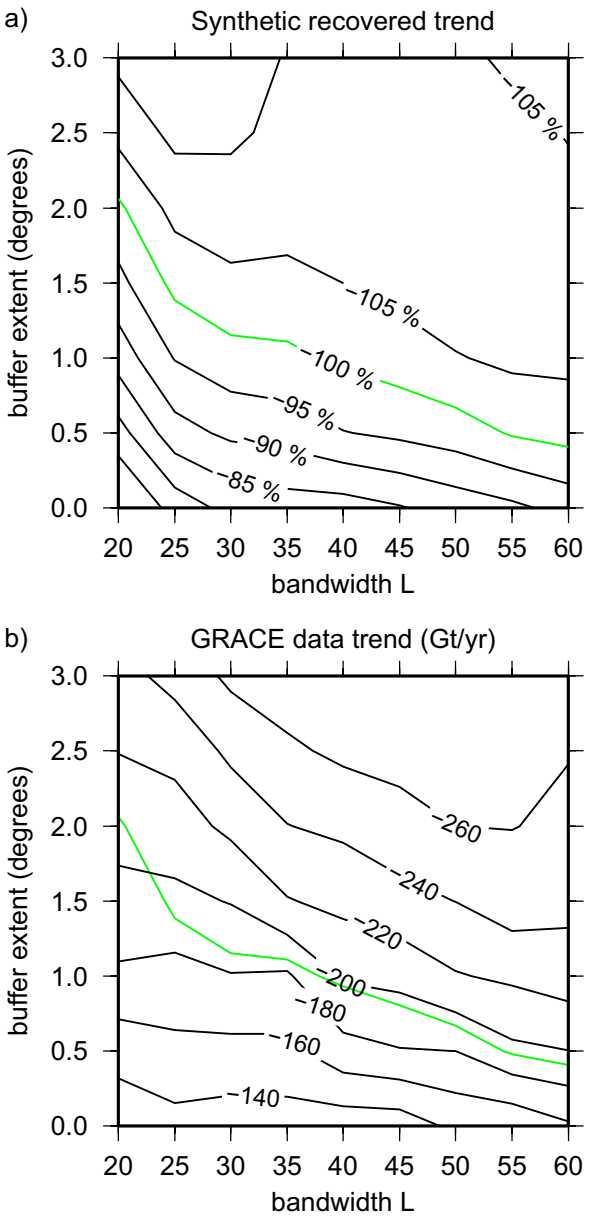


**Fig. S6.** The results of synthetic experiments to examine how recovered trends vary for different bandwidths (*L*) and different region buffers. (*A*) We place a uniform mass loss trend over the landmass of Greenland. To this trend, at each month, we add a realization of the noise from our residual covariance matrix. We then attempt to recover this trend for different bases over Greenland and report the normalized trend. (*B*) For the same bases, we report the trend recovered from the actual GRACE data in gigatons per year. Also drawn is the 100% recovery contour (*A*). We use this synthetic experiment to inform our preferred choice of a 0.5° buffer around Greenland.

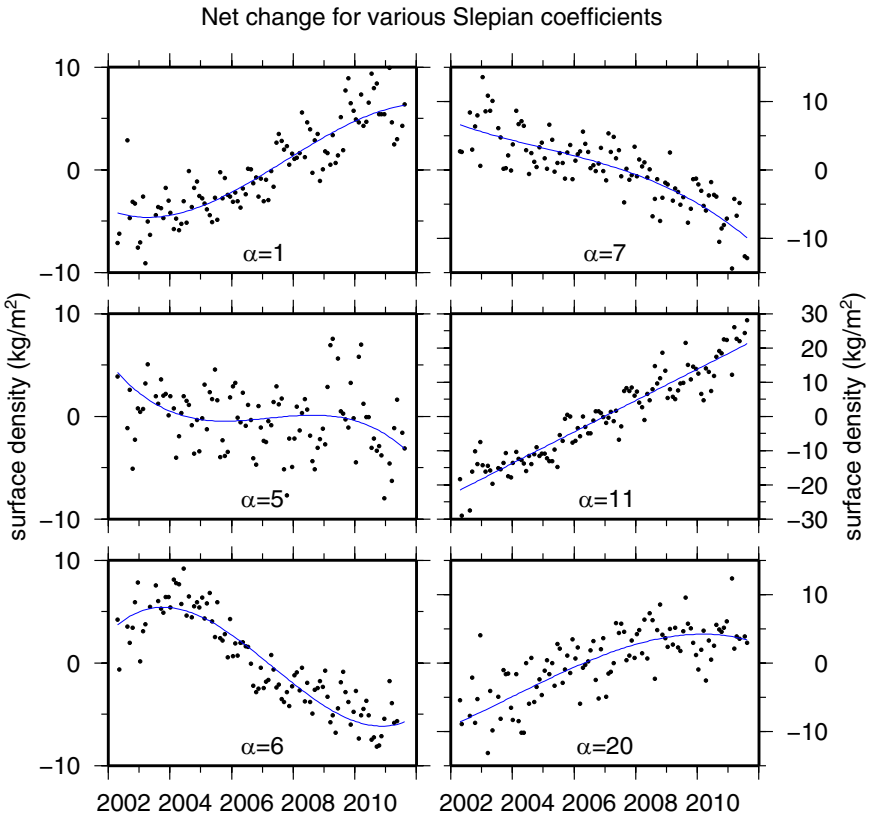


**Fig. S7.** Time series of various (α = 1, 5, 6, 7, 11, 20) Slepian coefficients and their best-fit polynomial (blue lines). Each coefficient is fit by an annual periodic and linear function as well as quadratic and cubic polynomial terms if those terms pass an *F* test for variance reduction. Shown here are the coefficient and fitted function values with the annual periodic function subtracted from both. The mean is removed from each time series.

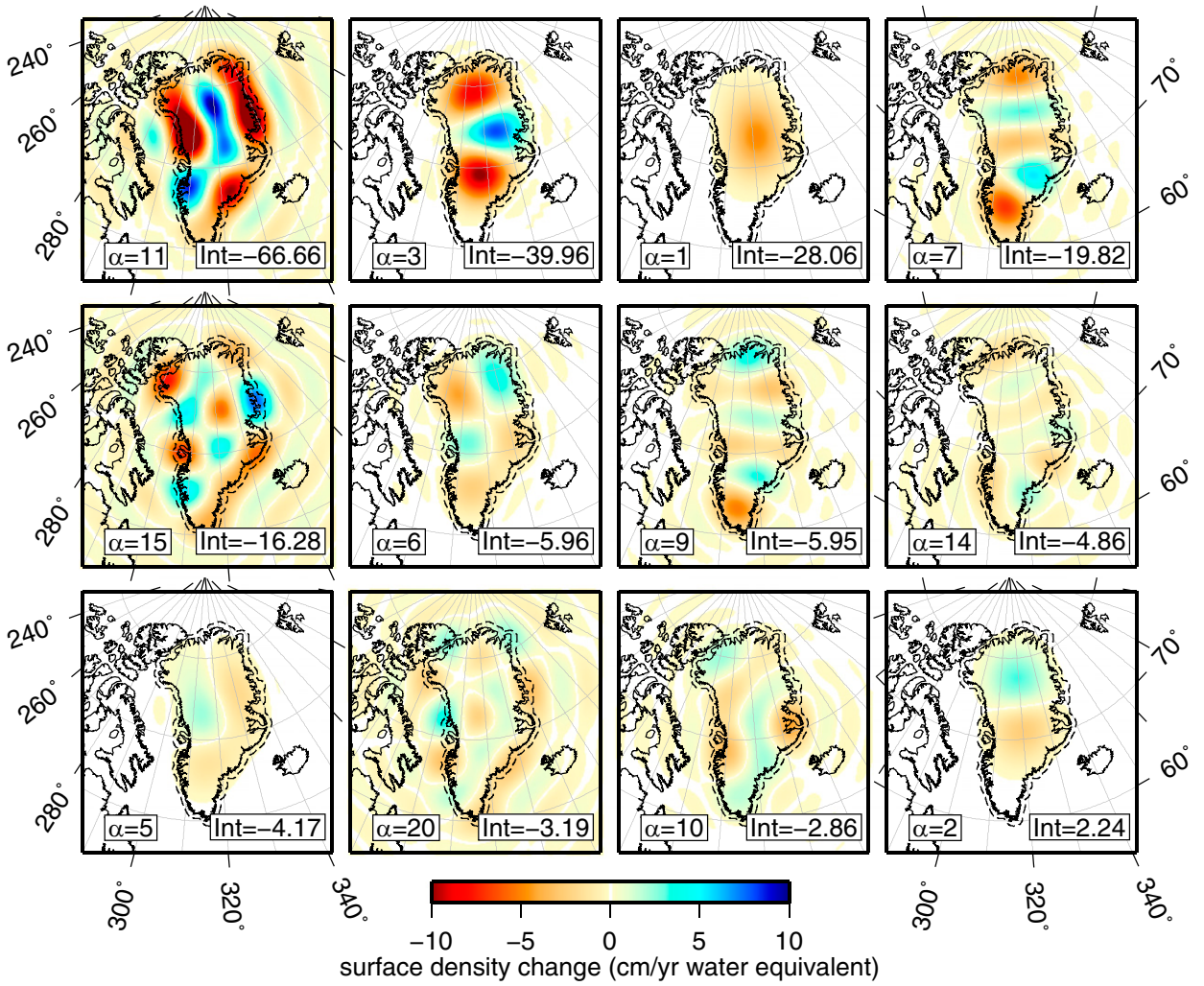


**Fig. S8.** Predicted GRACE annual mass change in the Slepian basis for each of the first 12 eigenfunctions. Each eigenfunction, denoted by its index α, is scaled by the total change in that coefficient from January of 2003 to November of 2011 divided by the time span (years) expressed as the centimeter per year water equivalent of surface density. Thus, this result represents the mass change for an average year during this time span. The variable Int displays the integral of each function in the concentration region within the dashed line expressed as the mass change rate of gigatons per year. Surface density change of absolute value smaller than 0.1 cm/y is left white.

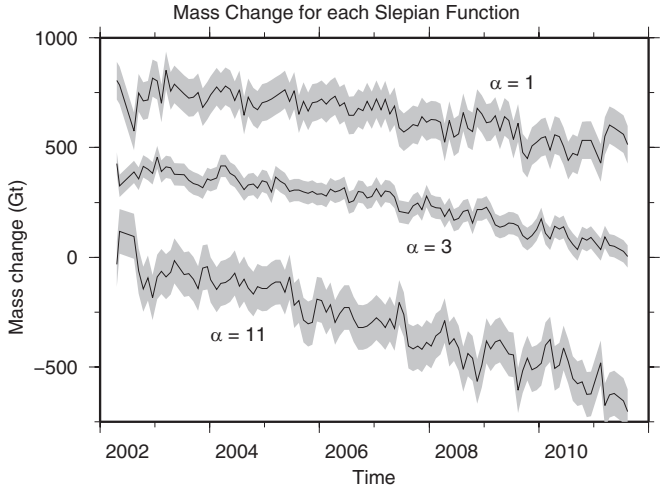


**Fig. S9.** Mass change in gigatons for the three most significant Slepian function terms (α = 1, 3, 11), which contribute more than 70% of total mass change over the data time span. Monthly data are drawn as the solid black lines, whereas the 2σ uncertainty envelopes are drawn in gray. Each function has a mean of zero but has been offset from zero for clarity.